How to cite: *Angew. Chem. Int. Ed.* **2022,** *61,* e202208163
International Edition: doi.org/10.1002/anie.202208163
German Edition: doi.org/10.1002/ange.202208163

Hydrogen Generation

sp-Carbon Incorporated Conductive Metal-Organic Framework as Photocathode for Photoelectrochemical Hydrogen Generation

Yang Lu[+], Haixia Zhong[+], Jian Li, Anna Maria Dominic, Yiming Hu, Zhen Gao, Yalong Jiao, Mingjian Wu, Haoyuan Qi, Chuanhui Huang, Lacey J. Wayment, Ute Kaiser, Erdmann Spiecker, Inez M. Weidinger, Wei Zhang, Xinliang Feng,* and Renhao Dong**

Abstract: Metal-organic frameworks (MOFs) have attracted increasing interest for broad applications in catalysis and gas separation due to their high porosity. However, the insulating feature and the limited active sites hindered MOFs as photocathode active materials for application in photoelectrocatalytic hydrogen generation. Herein, we develop a layered conductive two-dimensional conjugated MOF (2D c-MOF) comprising sp-carbon active sites based on arylene-ethynylene macrocycle ligand via CuO_4 linking, named as Cu_3HHAE_2. This sp-carbon 2D c-MOF displays apparent semiconducting behavior and broad light absorption till the near-infrared band (1600 nm). Due to the abundant acetylene units, the Cu_3HHAE_2 could act as the first case of MOF photocathode for photoelectrochemical (PEC) hydrogen generation and presents a record hydrogen-evolution photocurrent density of $\approx 260\ \mu A\ cm^{-2}$ at 0 V vs. reversible hydrogen electrode among the structurally-defined cocatalyst-free organic photocathodes.

Metal-organic frameworks (MOFs) are a class of porous crystalline coordination polymers consisting of metal ions/clusters and organic ligands,[1] and have exhibited great potential for the applications in gas storage and separation, catalysis, etc.[2] Recent advances reported that MOFs could also be utilized as cocatalysts and photosensitizers to mix with inorganic semiconductor nanomaterials for photoelectrochemical (PEC) hydrogen generation, due to their high porosity, structural diversity and tailorability, and ability to reduce electron-hole pair recombination.[3] However, the insulating feature and the limited active sites in traditional MOFs inevitably restrict their utilization as direct photocathode materials in PEC energy conversion.[4]

Generally, the photoelectrocatalysis efficiency is dominated by two fundamental processes: 1) semiconductors that absorb incident photons and generate photoexcited electron-hole pairs; 2) separation and migration of photogenerated excitons to the semiconductor surface.[5] Recently, two-dimensional conjugated MOFs (2D c-MOFs) have emerged as a unique class of layer-stacked materials; they exhibit

[*] Dr. Y. Lu,[+] Dr. H. Zhong,[+] A. M. Dominic, Dr. H. Qi, Dr. C. Huang, Prof. Dr. I. M. Weidinger, Prof. Dr. X. Feng, Dr. R. Dong
Center for Advancing Electronics Dresden & Faculty of Chemistry and Food Chemistry, Technische Universität Dresden
Mommsenstrasse 4, 01062 Dresden (Germany)
E-mail: xinliang.feng@tu-dresden.de
renhao.dong@tu-dresden.de

Dr. J. Li
Department of Fibre and Polymer Technology, KTH Royal Institute of Technology
Teknikringen 56, 10044 Stockholm (Sweden)

Y. Hu, L. J. Wayment, Prof. W. Zhang
Department of Chemistry, University of Colorado Boulder
Boulder, CO 80309 (USA)
E-mail: wei.zhang@colorado.edu

Z. Gao, Dr. Y. Jiao
College of Physics, Hebei Key Laboratory of Photophysics Research and Application, Hebei Normal University
Shijiazhuang 050024 (China)

Dr. M. Wu, Prof. Dr. E. Spiecker
Institute of Micro- and Nanostructure Research (IMN) & Center for Nanoanalysis and Electron Microscopy (CENEM), Interdisciplinary Center for Nanostructured Films (IZNF), Department of Materials Science and Engineering, Friedrich-Alexander-Universität Erlangen-Nürnberg
Cauerstrasse 3, 91058 Erlangen (Germany)

Dr. H. Qi, Prof. Dr. U. Kaiser
Central Facility of Materials Science Electron Microscopy, Universität Ulm
89081 Ulm (Germany)

Prof. Dr. X. Feng
Max Planck Institute for Microstructure Physics
06120 Halle (Saale) (Germany)

Dr. R. Dong
Key Laboratory of Colloid and Interface Chemistry of the Ministry of Education, School of Chemistry and Chemical Engineering, Shandong University
Jinan, 250100 (China)

[+] These authors contributed equally to this work.

intrinsic electrical conductivities (up to 10^3 S cm^{-1}), tunable band gaps (from metal to semiconductors), and excellent light-harvesting capabilities in the visible and near-infrared regions due to the inclusion of planar π-conjugated ligands and *d*-π-conjugated planar metal nodes.[6] Despite the great interest, 2D c-MOFs as direct photocathodes for PEC hydrogen generation have not been explored so far due to the lack of active sites. The currently reported 2D c-MOFs are exclusively composed of sp^2 hybridized carbon atoms that are not effective for assisting photogenerated exciton separation and migration.

Herein, we propose a design strategy and incorporate acetylene units (–C≡C–), known as efficient active sites for PEC hydrogen generation,[6i,7] into sp^2-carbon hybridized 2D c-MOFs. Thus, we develop the first sp-carbon embedded 2D c-MOF (Cu_3HHAE_2) single crystals via a coordination reaction between a hexahydroxyarylene-ethynylene macrocycle ligand (HHAE) and Cu^{2+} salt. According to the continuous rotation electron diffraction (cRED) and high-resolution transmission electron microscopy (HRTEM) analysis, Cu_3HHAE_2 exhibits a fully eclipsed layer stacking structure with an interlayer distance of 0.32 nm. Notably, the Cu_3HHAE_2 features a hierarchical pore structure with a kagome (**kgm**) geometry comprising hexagonal (2.20 nm) and triangular (0.30 nm) dual pores. The Cu_3HHAE_2 shows a broad light-harvesting capability with an optical gap of 0.87 eV and possesses the HOMO and LUMO levels of −5.26 eV and −4.39 eV, respectively, which are highly suitable for the PEC hydrogen evolution reaction (HER). Upon integration as a photocathode, the Cu_3HHAE_2 displays a high photocurrent density up to 260 μA cm^{-2} at 0 V vs. reversible hydrogen electrode (RHE), which is one of the highest among the cocatalyst-free organic photocathodes reported to date. By combining DFT calculations and electrochemical operando resonance Raman spectroscopy, we further demonstrate that the C≡C bonds serve as the active sites for hydrogen evolution. This work brings up a new design for unique acetylene functionalized dual-pore 2D c-MOF and demonstrates the possibility of 2D c-MOFs for highly-efficient photoelectrochemical catalytic conversions.

HHAE ligand was synthesized via acyclic diyne metathesis macrocyclization with a multidentate triphenolsilane-based Mo^{VI} carbyne complex as the catalyst, according to the literature.[7d] According to the DFT calculation, the incorporation of electron-deficient acetylene units could reduce the electron density at the metal-binding site, which would increase the acidity of the coordination group (–OH) and the reversibility of the metal-ligand bond during the MOF growth. (Figure S1).[8] In our optimized conditions, Cu_3HHAE_2 was synthesized under solvothermal conditions by reacting HHAE with $CuSO_4{\cdot}5H_2O$ in a 3:1 (v/v) H_2O and DMF in a glass vial at 85 °C for 12 hours (Figure 1a). Fourier-transform infrared (FT-IR) spectroscopy revealed the almost disappearance of the O–H stretching vibration band from the monomer HHAE in Cu_3HHAE_2 (Figure S2), demonstrating the successful coordination polymerization. Scanning electron microscopy (SEM, Figure 1b and Figure S3) showed hexagonal rods with a length of 1–5 μm.

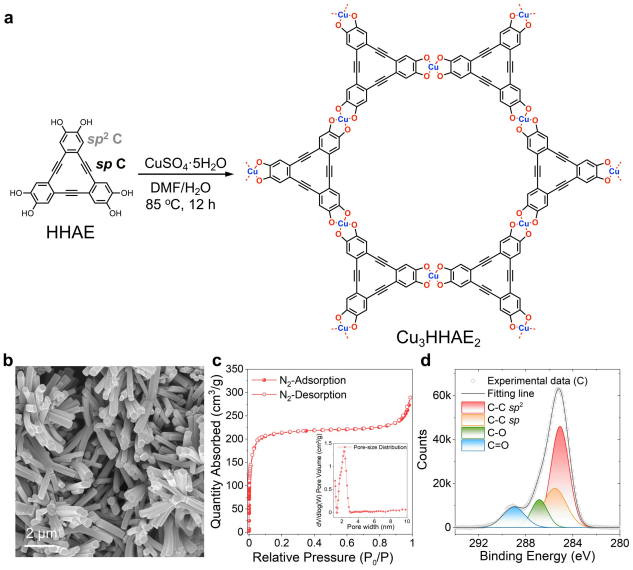

Figure 1. a) The synthetic scheme of Cu_3HHAE_2. b) SEM image of Cu_3HHAE_2. c) N_2 adsorption/desorption isotherms at 77.3 K and the corresponding pore size distribution in the inset. The high-resolution XPS scan of d) C 1s range (after etching) of Cu_3HHAE_2 MOF with area percentages of the deconvoluted peaks is given.

The porosity of Cu_3HHAE_2 was investigated by N_2 adsorption isotherms at 77 K. The sample activated by heating at 90 °C under a dynamic vacuum showed a Brunauer–Emmett–Teller (BET) surface area as high as 801 m^2 g^{-1} (Figure 1c). The stacked 2D sheets form 1D hexagonal channels with a pore diameter of ≈2.2 nm, which agrees with the average pore size of 2.16 nm obtained by fitting an N_2 adsorption isotherm to Cu_3HHAE_2. And the triangular pores located in the ligand are too small to be detected. X-ray photoelectron spectra (XPS) evidenced the presence of C, O, and Cu in the Cu_3HHAE_2 sample. The high-resolution analysis of the Cu 2p range confirmed a dominant distribution of Cu^{II} in the sample (Figure S4). The C 1s peaks of Cu_3HHAE_2 in Figure 1d can be deconvoluted into four subpeaks of C–C (sp^2) at 284.9 eV, C–C (sp) at 285.6 eV, C–O at 286.9 eV and C=O at 288.9 eV, respectively. The typical binding energy values of sp^2 and sp hybrid carbon atoms in Cu_3HHAE_2 are consistent with other sp-carbon embedded organic conjugated materials.[9] XPS data show that the samples have both sp^2 and sp hybrid carbon atoms, and the area ratio of the two peaks is close to 2:1, consistent with the chemical structure of Cu_3HHAE_2. Furthermore, the nearly 1:1 distribution of C–O and C=O is observed in Cu_3HHAE_2, which is consistent with the reported 2D c-MOFs with [CuO_4] secondary building units (SBUs).[10] Thermogravimetric analysis (TGA) showed that Cu_3HHAE_2 started desolvation over 100 °C and likely decomposition above 180 °C (Figure S5).

The continuous rotation electron diffraction (cRED) technique was performed on Cu_3HHAE_2 single crystals to determine its exact structure.[11] The cRED data showed hexagonal symmetry for Cu_3HHAE_2, and the structure solution revealed that Cu^{2+} cations possess square-planar

coordination, forming square-planar [CuO_4] units with two HHAE ligands. Each trigonal HHAE ligand is further surrounded by three [CuO_4] units to form an infinite planar 2D layer with a honeycomb-like arrangement ($a=b=$ 26.54 Å). Cu_3HHAE_2 possessed a short interlayer distance of 3.21 ± 0.02 Å and a perfect π–π stacking between the HHAE ligands (Figure 2a,b, Figure S6). Powder X-ray diffraction (PXRD) analysis of Cu_3HHAE_2 revealed a crystalline structure with prominent peaks at $2\theta=3.8°$, 7.6°, and 10.1°, corresponding to the (100), (200), and (210) reflections, respectively (Figure 2c). In addition, the peak at $2\theta=27.9°$ refers to the π–π stacking (001) reflections. The perfect eclipsed stacking structure of Cu_3HHAE_2 was further confirmed by Rietveld refinement against PXRD, which converged with $R_p=3.04\,\%$, and $R_{wp}=5.18\,\%$ (Figure 2c). The experimental data of PXRD perfectly agrees with the calculated XRD pattern, which confirms the high phase purity of the Cu_3HHAE_2 sample. High-resolution transmission electron microscopy (HRTEM) of a tiny crystallite oriented close to the (001) zone axis (Figure 2d) allowed direct imaging of the honeycomb-like porous network with $a=b=26.2$ Å and $\gamma=120°$, which agrees well with the single-crystal analysis. Furthermore, the experimental elastically filtered selection area electron diffraction also presented a perfect agreement with the simulation using the structural model derived above (Figure 2e). It should be noticed that Cu_3HHAE_2 is the first case of a kagome 2D c-MOF with a hierarchical dual-pore structure. The diameters for the hexagonal and triangle pore are determined as 2.2 and 0.3 nm, respectively.

The four-probe van der Pauw measurements under vacuum indicated the electrical conductivities at 298 K of the powder pellets as $2.40\times10^{-4}\,S\,m^{-1}$ for Cu_3HHAE_2 (Figure 3a). As shown in Figure 3b, Cu_3HHAE_2 presents thermally-activated charge transport according to the variable-temperature (VT) conductivity measurements from 200 to 320 K with a hopping activation energy of 0.41 eV, which revealed an apparent semiconducting behavior in Cu_3HHAE_2. The Vis-NIR spectra of Cu_3HHAE_2 present two kinds of broad absorption bands till 1600 nm. The optical gap estimated from the onset of the near-infrared region and Tauc plots was ≈0.87 eV (Figure 3c and Figure S7), further suggesting the semiconducting property of bulk Cu_3HHAE_2. Figure 3d and Figure S8 show the ultraviolet photoelectron spectra (UPS) of Cu_3HHAE_2, recorded in both the secondary electron cutoff region (SECO) and the low binding energy region of the highest occupied molecular orbital (HOMO) region.[12] The Fermi level and HOMO level of Cu_3HHAE_2 are located at −4.60 and −5.26 eV, respectively. Combined with the UV-derived optical band gap, the LUMO level of Cu_3HHAE_2 was estimated to be −4.39 eV. In comparison to the energy level of the H_2O/H_2 redox pair (−4.44 eV), the higher-lying

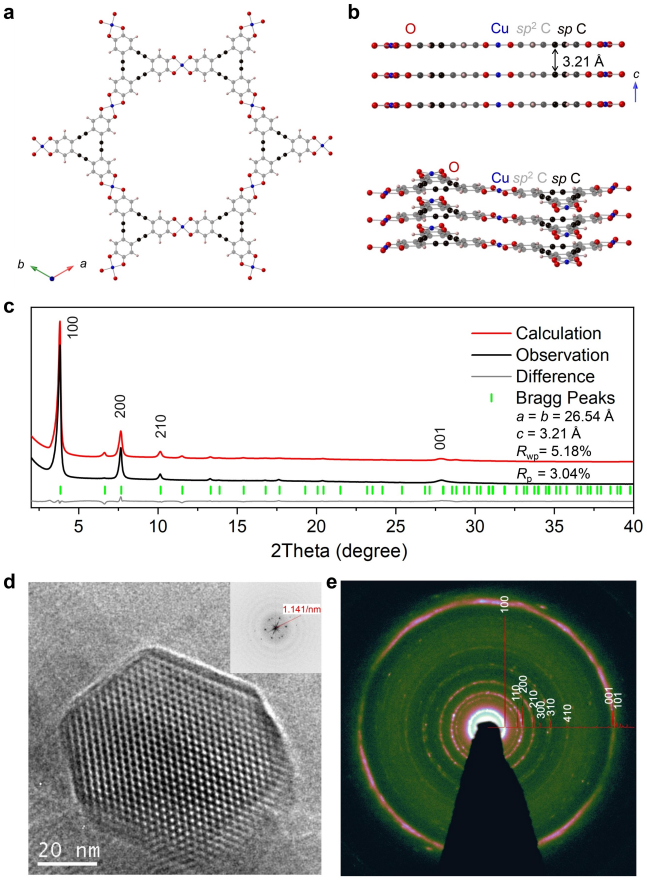

Figure 2. a) A portion of the crystal structure along the c direction. b) Views parallel to the ab plane. Single-crystal structure derived from cRED. c) Overlay of the experimental and Rietveld refinement plots of Cu_3HHAE_2, with profile, weighted profile fitting factors $R_p=3.04\,\%$, $R_{wp}=5.81\,\%$, respectively. d) HRTEM image of a Cu_3HHAE_2 (inset: FFT). e) Zero-loss filtered selection area electron diffraction (SAED) pattern of Cu_3HHAE_2 with simulated powder pattern superimposed.

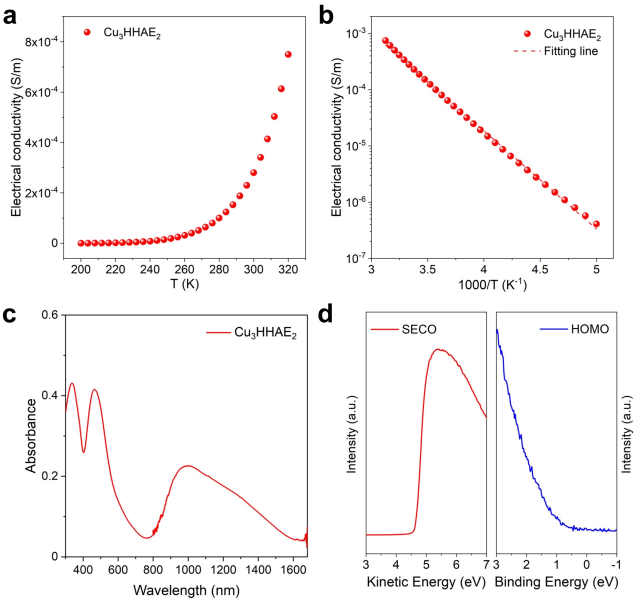

Figure 3. a,b) variable-temperature electrical conductivities of Cu_3HHAE_2. c) Vis-NIR absorption spectroscopy of Cu_3HHAE_2. d) UPS results of Cu_3HHAE_2; the left image is the low kinetic energy region of UPS spectra, and the right image is the low binding energy region (HOMO).

LUMO levels suggest that Cu_3HHAE_2 is a potential candidate for the transfer of photoexcited electrons to H^+ for H_2 evolution.

According to the detailed characterization of the chemical structure and optoelectronic properties, Cu_3HHAE_2 can serve as a promising cocatalyst-free organic photocathode to potentially enhance the performance of PEC HER due to its broad light-harvesting ability and the abundant embedded acetylene as the promising active sites to assist the photogenerated exciton migration. To validate this concept, PEC HER measurement was performed using a three-electrode electrochemical cell with the prepared Cu_3HHAE_2 or HHAE monomer on Cu foam as working electrode, Ag/AgCl (sat.) as reference electrode, and graphite rode as counter electrode in 0.1 M Na_2SO_4 electrolyte. The linear sweep voltammetry curves recorded under dark and solar irradiation (Figure S9) revealed the apparent photocurrent response of these samples, wherein the recorded dark current density originated from the capacitive behavior of the catalysts and Cu foam current collector. Cu_3HHAE_2 cathode exhibited a more significant photocurrent density up to $\approx 260\ \mu A\,cm^{-2}$ recorded at 0 V vs. RHE (Figure 4a), which was 2.6 higher than that of HHAE ($\approx 100\ \mu A\,cm^{-2}$) and among the state-of-art cocatalyst-free organic photocathodes like graphdiyne, carbon nitride, covalent organic frameworks, polymers, and organic heterojunction, etc. (< 100 uA cm^{-2}, Table S1).[7a,e,i,13] Of note, no obvious photocurrent was detected for the Cu foam substrate under identical condition, suggesting that the photocurrent of Cu_3HHAE_2 cathode originates from the Cu_3HHAE_2 MOF (Figure 4a).

Besides, the higher intrinsic PEC performance of Cu_3HHAE_2 was gleaned from its larger peak incident-photon-to-current efficiency (IPCE) value (0.75 % at 480 nm) compared to HHAE (0.28 % at 420 nm) at 0 V vs. RHE (Figure 4b and Figure S10). Next, the electrochemical impedance analysis was carried out to investigate the charge-transfer resistance of Cu_3HHAE_2. As shown in Figure 4c, all these electrodes showed a reduced charge-transfer resistance under light illumination, which is associated with the photoinduced charge carriers under light illumination. Due to the lack of in-plane d-π conjugated transport channels, the HHAE cathode exhibited a higher charge-transfer resistance than Cu_3HHAE_2. These results demonstrated the synergistic contribution of conjugated acetylenic structure and efficient charge transfer pathway to boosting the PEC HER performance of Cu_3HHAE_2 photocathode. Accordingly, the carrier-separation efficiency of Cu_3HHAE_2 was calculated to be 0.09 %, which is higher than HHAE (0.005 %) (Figure 4d). Thus, a 2D conjugated framework with large acetylenic and metal complexes centers afford Cu_3HHAE_2 2D c-MOF with superior PEC HER performance. Furthermore, the long-term durability of Cu_3HHAE_2 was estimated (Figure S11). Cu_3HHAE_2 exhibited good stability as only a slight decrease of the photocurrent density was observed for Cu_3HHAE_2 after more than 32 hours of solar light irradiation at 0 V vs. RHE, which was likely due to the peeling off of the catalyst from Cu foam induced by the hydrogen evolution. The ex situ SEM, elemental mapping, XRD, XPS, FT-IR, and Raman spectrum analysis after the long-term test (Figures S2, S11–14) verified the stable chemical states and crystalline structure of Cu_3HHAE_2.

To verify the role of the sp carbons of Cu_3HHAE_2 in PEC HER, operando electrochemical-Raman spectroscopy was carried out using an excitation laser line of 594 nm to trace the alterations of acetylene bond strength during the PEC HER. The intrinsic Raman signal (at the open circuit potential) of sp carbons in Cu_3HHAE_2 was shown at 2116 cm^{-1}, which is the typical vibration of sp carbons.[7e,i] As the cathodic current density of Cu_3HHAE_2 gradually increased in a potential scan from 0.7 to 0.0 V vs. RHE, the intensity of the C≡C bond vibrational mode at 2116 cm^{-1} decreased, and a new broadband correspondingly arose at 2044 cm^{-1} (Figure 5a, Figure S9c). Notably, the band at 2044 cm^{-1} reversibly disappeared upon the increase of the

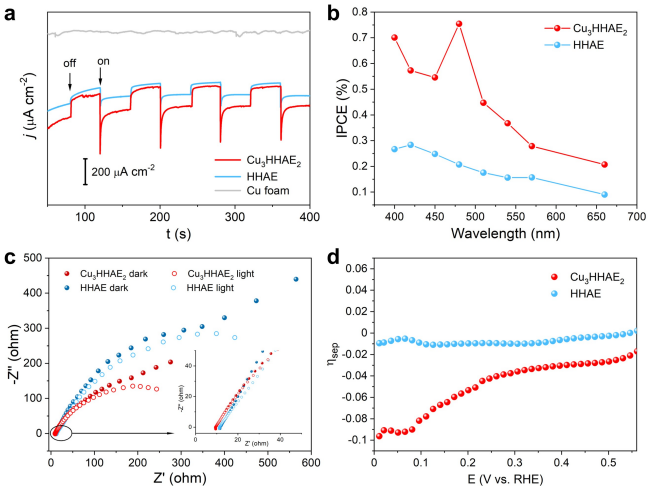

Figure 4. a) Photocurrent-time plots for Cu_3HHAE_2 and HHAE cathodes at 0 V vs. RHE. On: illumination on; off: illumination off. b) IPCE of Cu_3HHAE_2 and HHAE cathodes under AM 1.5G irradiation. c) Potentiostatic electrochemical impedance spectroscopy (PEIS) plots of Cu_3HHAE_2 and HHAE cathodes at 0 V vs. RHE with and without light irradiation. The inset is the enlarged image. d) Carrier-separation efficiency (η_{sep}) of Cu_3HHAE_2 and HHAE cathodes under different applied potentials.

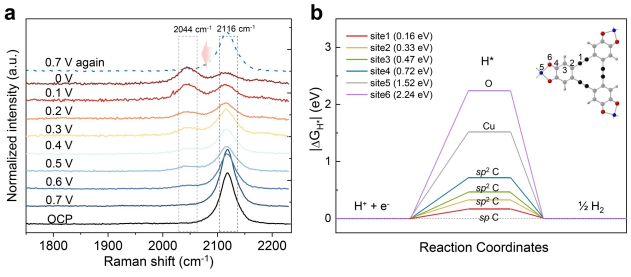

Figure 5. a) Potential-dependent Raman spectra of Cu_3HHAE_2 in 0.1 M Na_2SO_4 under 594 nm laser excitation (OCP, open circuit potential). Operando resonance Raman spectra. b) Free-energy diagram for H_2-evolution via a single-site reaction pathway: 1, 2, 3, 4, 5, 6 denote different active sites of Cu_3HHAE_2.

potential to 0.7 V vs. RHE, thus assigning it to a transient state of C≡C bonds during the PEC HER process. The shift of the transient Raman active vibration from 2116 to 2044 cm^{-1} indicates a decrease in the bond strength of the C≡C bond induced by external potential and light irradiation.[14] This activated state with enhanced electron density in the antibonding orbital is ideally suited to act as a highly active center for proton adsorption enabling subsequent HER process.[7g]

Then, we performed the theoretical calculation to further investigate the hydrogen evolution mechanism, including eight different structural sites and their following HER process (Figure 5b). In order to be an ideal catalyst for HER, the absolute value of Gibbs free energy should be close to 0 eV.[15] A section of the pore wall consisting of one full ligand and three half SBUs was cut from the single-crystal structures and further used for calculations. Indeed, site 1 exhibits a lower absolute value of ΔG_{H^*}(0.17 eV) compared to sites 2–4 (ΔG_{H^*}: 0.33, 0.47, and 0.72 eV), indicating fast HER kinetics on sp carbons. Moreover, the Cu (site 5) and the O (site 6) in SBUs display high free energies for H* formation of 1.52 and 2.24 eV, respectively. Thus, the calculation results further support that the –C≡C– bonds in Cu_3HHAE_2 serve as the active sites for PEC HER.

In conclusion, we reported the first acetylene-containing 2D c-MOF based on the hexahydroxyarylene-ethynylene macrocycle ligand. The chemical structure of Cu_3HHAE_2 single crystals was elucidated by cRED at the atomic level. Cu_3HHAE_2 exhibits a kagome (**kgm**) geometry with unique dual-pore structures at the atomic scale. The optoelectronic property studies indicated the apparent semiconducting feature of the MOF with the optical band gap of 0.87 eV, largely due to the localized feature of cross-conjugation acetylene bonds. The conductive MOF embedded with sp-hybridized carbon displayed an excellent photocurrent density up to 260 $\mu A\,cm^{-2}$, which is the first case of conductive MOF as the direct cathode material for PEC hydrogen generation. DFT calculations and operando Raman measurements proved that the active sites actually originated from the acetylene units. This work provides a reliable structure-photoelectrochemical property relationship for a unique sp-carbon incorporated MOF and will drive the discovery of conductive MOFs for various photoelectrochemical conversion applications.

Acknowledgements

The authors acknowledge cfaed and Dresden Center for Nano-analysis (DCN) at TUD. This work is financially supported by ERC starting grant (FC2DMOF, No. 852909), EU Graphene Flagship (Core3, No. 881603), ERC Consolidator Grant (T2DCP), DFG projects (SFB-1415, No. 417590517; SPP 1928, COORNET), EMPIR-20FUN03-COMET, H2020-FETOPEN-PROGENY (No. 899205) as well as the German Science Council and Center of Advancing Electronics Dresden (cfaed). R.D. thanks Taishan Scholars Program of Shandong Province (tsqn201909047). I.W. acknowledges the cluster of excellence UniSysCat (EXC 2008/1-390540038). W.Z. thanks the support from National Science Foundation (CHE-2108197). Open Access funding enabled and organized by Projekt DEAL.

Conflict of Interest

The authors declare no conflict of interest.

Data Availability Statement

The data that support the findings of this study are available from the corresponding author upon reasonable request.

Keywords: Conductive 2D MOFs · Hydrogen Generation · Photocathode · Photoelectrocatalysis · sp-Carbon

[1] O. M. Yaghi, M. J. Kalmutzki, C. S. Diercks, *Introduction to reticular chemistry: metal–organic frameworks and covalent organic frameworks*, Wiley, Hoboken, **2019**.

[2] a) C. A. Trickett, A. Helal, B. A. Al-Maythalony, Z. H. Yamani, K. E. Cordova, O. M. Yaghi, *Nat. Rev. Mater.* **2017**, *2*, 17045; b) H.-C. Zhou, S. Kitagawa, *Chem. Soc. Rev.* **2014**, *43*, 5415–5418; c) E. A. Dolgopolova, A. M. Rice, C. R. Martin, N. B. Shustova, *Chem. Soc. Rev.* **2018**, *47*, 4710–4728; d) M. Zhao, Y. Huang, Y. Peng, Z. Huang, Q. Ma, H. Zhang, *Chem. Soc. Rev.* **2018**, *47*, 6267–6295; e) H. Zhang, J. Li, Q. Tan, L. Lu, Z. Wang, G. Wu, *Chem. Eur. J.* **2018**, *24*, 18137–18157.

[3] a) A. Dhakshinamoorthy, A. M. Asiri, H. Garcia, *Angew. Chem. Int. Ed.* **2016**, *55*, 5414–5445; *Angew. Chem.* **2016**, *128*, 5504–5535; b) B. Xia, Y. Yang, Y. Zhang, Y. Xia, M. Jaroniec, J. Yu, J. Ran, S.-Z. Qiao, *Chem. Eng. J.* **2022**, *431*, 133944; c) E. Zhao, K. Du, P. F. Yin, J. Ran, J. Mao, T. Ling, S. Z. Qiao, *Adv. Sci.* **2022**, *9*, 2104363.

[4] V. Stavila, A. A. Talin, M. D. Allendorf, *Chem. Soc. Rev.* **2014**, *43*, 5994–6010.

[5] a) T. Hisatomi, J. Kubota, K. Domen, *Chem. Soc. Rev.* **2014**, *43*, 7520–7535; b) S. J. A. Moniz, S. A. Shevlin, D. J. Martin, Z.-X. Guo, J. Tang, *Energy Environ. Sci.* **2015**, *8*, 731–759.

[6] a) M. Wang, R. Dong, X. Feng, *Chem. Soc. Rev.* **2021**, *50*, 2764–2793; b) L. S. Xie, G. Skorupskii, M. Dinca, *Chem. Rev.* **2020**, *120*, 8536–8580; c) M. Ko, L. Mendecki, K. A. Mirica, *Chem. Commun.* **2018**, *54*, 7873–7891; d) M. S. Yao, X. J. Lv, Z. H. Fu, W. H. Li, W. H. Deng, G. D. Wu, G. Xu, *Angew. Chem. Int. Ed.* **2017**, *56*, 16510–16514; *Angew. Chem.* **2017**, *129*, 16737–16741; e) X. Huang, P. Sheng, Z. Tu, F. Zhang, J. Wang, H. Geng, Y. Zou, C. A. Di, Y. Yi, Y. Sun, W. Xu, D. Zhu, *Nat. Commun.* **2015**, *6*, 7408–7415; f) A. J. Clough, J. W. Yoo, M. H. Mecklenburg, S. C. Marinescu, *J. Am. Chem. Soc.* **2015**, *137*, 118–121; g) D. Feng, T. Lei, M. R. Lukatskaya, J. Park, Z. Huang, M. Lee, L. Shaw, S. Chen, A. A. Yakovenko, A. Kulkarni, J. Xiao, K. Fredrickson, J. B. Tok, X. Zou, Y. Cui, Z. Bao, *Nat. Energy* **2018**, *3*, 30–36; h) J. Liu, X. Song, T. Zhang, S. Liu, H. Wen, L. Chen, *Angew. Chem. Int. Ed.* **2021**, *60*, 5612–5624; *Angew. Chem.* **2021**, *133*, 5672–5684; i) R. Dong, M. Pfeffermann, H. Liang, Z. Zheng, X. Zhu, J. Zhang, X. Feng, *Angew. Chem. Int. Ed.* **2015**, *54*, 12058–12063; *Angew. Chem.* **2015**, *127*, 12226–12231.

[7] a) H. Sun, I. H. Oner, T. Wang, T. Zhang, O. Selyshchev, C. Neumann, Y. Fu, Z. Liao, S. Xu, Y. Hou, A. Turchanin, D. R. T. Zahn, E. Zschech, I. M. Weidinger, J. Zhang, X. Feng,

Angew. Chem. Int. Ed. **2019**, *58*, 10368–10374; *Angew. Chem.* **2019**, *131*, 10476–10482; b) P. Pachfule, A. Acharjya, J. Roeser, T. Langenhahn, M. Schwarze, R. Schomacker, A. Thomas, J. Schmidt, *J. Am. Chem. Soc.* **2018**, *140*, 1423–1427; c) J. W. Crowe, L. A. Baldwin, P. L. McGrier, *J. Am. Chem. Soc.* **2016**, *138*, 10120–10123; d) H. Yang, Y. Du, S. Wan, G. D. Trahan, Y. Jin, W. Zhang, *Chem. Sci.* **2015**, *6*, 4049–4053; e) M. Borrelli, C. J. Querebillo, D. L. Pastoetter, T. Wang, A. Milani, C. Casari, H. Khoa Ly, F. He, Y. Hou, C. Neumann, A. Turchanin, H. Sun, I. M. Weidinger, X. Feng, *Angew. Chem. Int. Ed.* **2021**, *60*, 18876–18881; *Angew. Chem.* **2021**, *133*, 19025–19031; f) H. Zhong, M. Ghorbani-Asl, K. H. Ly, J. Zhang, J. Ge, M. Wang, Z. Liao, D. Makarov, E. Zschech, E. Brunner, I. M. Weidinger, J. Zhang, A. V. Krasheninnikov, S. Kaskel, R. Dong, X. Feng, *Nat. Commun.* **2020**, *11*, 1409–1418; g) S. Ghosh, N. A. Kouame, L. Ramos, S. Remita, A. Dazzi, A. Deniset-Besseau, P. Beaunier, F. Goubard, P. H. Aubert, H. Remita, *Nat. Mater.* **2015**, *14*, 505–511; h) H. Sun, C. Dong, Q. Liu, Y. Yuan, T. Zhang, J. Zhang, Y. Hou, D. Zhang, X. Feng, *Adv. Mater.* **2020**, *32*, 2002486; i) H. Sun, C. Neumann, T. Zhang, M. Loffler, A. Wolf, Y. Hou, A. Turchanin, J. Zhang, X. Feng, *Adv. Mater.* **2019**, *31*, 1900961.

[8] J. H. Dou, M. Q. Arguilla, Y. Luo, J. Li, W. Zhang, L. Sun, J. L. Mancuso, L. Yang, T. Chen, L. R. Parent, G. Skorupskii, N. J. Libretto, C. Sun, M. C. Yang, P. V. Dip, E. J. Brignole, J. T. Miller, J. Kong, C. H. Hendon, J. Sun, M. Dinca, *Nat. Mater.* **2021**, *20*, 222–228.

[9] Y. Hu, C. Wu, Q. Pan, Y. Jin, R. Lyu, V. Martinez, S. Huang, J. Wu, L. J. Wayment, N. A. Clark, M. B. Raschke, Y. Zhao, W. Zhang, *Nat. Synth.* **2022**, *1*, 449–454.

[10] Z. Meng, C. G. Jones, S. Farid, I. U. Khan, H. M. Nelson, K. A. Mirica, *Angew. Chem. Int. Ed.* **2022**, *61*, e202113569; *Angew. Chem.* **2022**, *134*, e202113569.

[11] Z. Huang, E. S. Grape, J. Li, A. K. Inge, X. Zou, *Coord. Chem. Rev.* **2021**, *427*, 213583–213596.

[12] D. Huang, H. Yao, Y. Cui, Y. Zou, F. Zhang, C. Wang, H. Shen, W. Jin, J. Zhu, Y. Diao, W. Xu, C. A. Di, D. Zhu, *J. Am. Chem. Soc.* **2017**, *139*, 13013–13023.

[13] a) Y.-Y. Han, X.-L. Lu, S.-F. Tang, X.-P. Yin, Z.-W. Wei, T.-B. Lu, *Adv. Energy Mater.* **2018**, *8*, 1702992; b) S. Xu, H. Sun, M. Addicoat, B. P. Biswal, F. He, S. Park, S. Paasch, T. Zhang, W. Sheng, E. Brunner, Y. Hou, M. Richter, X. Feng, *Adv. Mater.* **2021**, *33*, 2006274.

[14] A. Shimojima, H. Takahashi, *J. Phys. Chem.* **1993**, *97*, 9103–9112.

[15] J. Mou, Y. Gao, J. Wang, J. Ma, H. Ren, *RSC Adv.* **2019**, *9*, 11755–11761.

Manuscript received: June 2, 2022
Accepted manuscript online: July 29, 2022
Version of record online: August 24, 2022